Dnmt3a1 regulates hippocampus-dependent memory via the downstream target Nrp1

Janina Kupke[1,2], Julien Klimmt[1,3,#], Franziska Mudlaff[1,4,#], Maximilian Schwab[1,5], Pavlo Lutsik[6,7], Christoph Plass[6], Carsten Sticht[8] and Ana M.M. Oliveira[1,9,*]

[1]Department of Neurobiology, Interdisciplinary Center for Neurosciences (IZN), Heidelberg University, 69120 Heidelberg, Germany

[2]Present address: Department of Molecular and Cellular Neurobiology, Center for Neurogenomics and Cognitive Research, Vrije Universiteit Amsterdam, 1081 HV, Netherlands

[3]Present address: Institute for Stroke and Dementia Research, University Hospital, Ludwig-Maximilians-University Munich, 81377 Munich, Germany

[4]Present address: Integrated Program in Neuroscience, McGill University, Montreal, QC H3A 2B4, Canada; Centre for Research in Neuroscience, Research Institute of the McGill University Health Centre, Montreal QC, H3G 1A4, Canada

[5]Present address: Department of Medical Oncology, National Center for Tumor Diseases (NCT) Heidelberg, University Hospital Heidelberg, 69120 Heidelberg, Germany

[6]Division of Cancer Epigenomics, German Cancer Research Center (DKFZ), 69120 Heidelberg, Germany

[7]Department of Oncology, KU Leuven, 3000 Leuven, Belgium

[8]Next Generation Sequencing Core Facility, Medical Faculty Mannheim, Heidelberg University, 68167, Mannheim, Germany

[9]Department of Molecular and Cellular Cognition Research, Central Institute of Mental Health, Medical Faculty Mannheim, Heidelberg University, 68159 Mannheim, Germany

[#]equal contribution

*Ana M.M. Oliveira. Department of Molecular and Cellular Cognition Research, Central Institute of Mental Health, Medical Faculty Mannheim, Heidelberg University, 68159 Mannheim, Germany. Phone: +49(0)62215416510. Email: oliveira@nbio.uni-heidelberg.de, ana.oliveira@zi-manheim.de

Abstract

Epigenetic factors are well established players in memory formation. Specifically, DNA methylation is necessary for the formation of long-term memory in multiple brain regions including the hippocampus. Despite the demonstrated role for DNA methyltransferases (Dnmts) in memory formation, it is unclear whether individual Dnmts have unique or redundant functions in long-term memory formation. Furthermore, the downstream processes controlled by Dnmts during memory consolidation have not been investigated. In this study, we demonstrated that Dnmt3a1, the predominant Dnmt in the adult brain, is required for long-term spatial object recognition and contextual fear memory. Using RNA-sequencing, we identified an activity-regulated Dnmt3a1-dependent genomic program in which several genes were associated with functional and structural plasticity. Furthermore, we found that some of the identified genes are selectively dependent on Dnmt3a1, but not its isoform Dnmt3a2. Specifically, we identified Neuropilin 1 (Nrp1) as a downstream target of Dnmt3a1 and further demonstrated the involvement of Nrp1 in hippocampus-dependent memory formation. Importantly, we found that Dnmt3a1 regulates hippocampus-dependent memory via Nrp1. In contrast, Nrp1 overexpression did not rescue memory impairments triggered by reduced Dnmt3a2 levels. Taken together, our study uncovered a Dnmt3a-isoform-specific mechanism in memory formation, identified a novel regulator of memory, and further highlighted the complex and highly regulated functions of distinct epigenetic regulators in brain function.

63 **Introduction**

64

65 Precise control of gene transcription is required for the functional and structural neuronal
66 remodelling that underlies memory formation and maintenance(1–3). Gene transcription is
67 orchestrated by the activity of transcription factors(4,5), epigenetic factors, and 3D-genomic
68 factors such as chromatin structure or nuclear organization(6–9). Indeed, epigenetic
69 mechanisms such as DNA methylation have emerged as important regulators of cognitive
70 processes(8).

71 DNA methylation has traditionally been viewed as a static mechanism with important roles in
72 transcription repression, cell fate determination, imprinting and silencing of transposons during
73 early development (10). However, it is now well accepted that DNA methylation plays a critical
74 role in the regulation of genomic responses in mature neurons. Several lines of evidence
75 demonstrated dynamic and quick changes in DNA methylation in response to neuronal
76 activity(11,12) and pharmacological and genetic studies established a causal link between
77 DNA methyltransferase (Dnmt) activity and memory formation. Specifically, the *de novo* DNA
78 methyltransferase, Dnmt3a, plays a documented function in cognitive abilities(13–17).
79 Furthermore, it has recently been shown that *DNMT3A* variants are the underlying cause of
80 the neurodevelopmental disorder Tatton-Brown-Rahman syndrome, which is characterized by
81 intellectual disability(18,19). Despite this evidence, the downstream processes regulated by
82 Dnmt3a that contribute to memory formation are unknown. Moreover, the genomic program
83 regulated by Dnmt3a and required for the formation of long-term memory remains uncovered.

84 The Dnmt3a genomic locus gives rise to two isoforms, Dnmt3a1 and Dnmt3a2(20), that exhibit
85 different genomic binding(21) and expression regulation in response to neuronal activity.
86 Dnmt3a2 is transcribed from an intronic promoter and behaves like an immediate early gene,
87 whereas the expression of Dnmt3a1 is not regulated at the level of transcription by neuronal
88 activity(22–24). The requirement for Dnmt3a2 in memory formation has been
89 demonstrated(23–25); however, the contribution of Dnmt3a1, despite its high abundance in

90 the adult brain(26–28) has not been investigated. The differential regulation of expression of
91 the two isoforms by neuronal activity and the studies that showed that normal Dnmt3a1
92 expression levels do not compensate the memory impairments found in Dnmt3a2 knockdown
93 mice (23,24,29,30), suggest nonredundant functions by the two isoforms. However, whether
94 the two enzymes are differentially required for and regulate distinct downstream processes
95 during memory formation remains to be investigated.

96 In this study, we demonstrated that Dnmt3a1 is crucial for memory formation and for
97 controlling an activity-regulated genomic program. We found that acute hippocampal reduction
98 of Dnmt3a1 led to memory impairments in adult mice in the spatial object recognition test and
99 contextual fear conditioning tasks without affecting hippocampus-independent tasks.
100 Moreover, using RNA Sequencing analysis, we identified activity-regulated genes dependent
101 on Dnmt3a1 levels. Intriguingly, we found that some of the identified genes are selectively
102 dependent on Dnmt3a1, but not Dnmt3a2. Among these genes was Neuropilin-1 (Nrp1), a
103 member of the semaphorin complex with an established function in synaptic plasticity(31,32).
104 In a next step, we demonstrated the involvement of Nrp1 in long-term spatial object recognition
105 and contextual fear memories. Furthermore, we showed that Dnmt3a1 regulates
106 hippocampus-dependent memory via Nrp1. In contrast, Nrp1 overexpression did not rescue
107 memory impairments triggered by reduced Dnmt3a2 levels, suggesting an isoform-specific
108 mechanism for memory processes. Taken together these findings uncovered a Dnmt3a1-
109 dependent genomic program and identified a downstream effector during memory formation.

110

111

112 **Materials and Methods**

113

114 Animals.

115 3-month-old C57BL/6N male mice (Charles River, Sulzfeld, Germany) were used and housed
116 2-3 per cage (except during severe fighting) with *ad libitum* access to water and food, under

117 a 12h light/dark cycle at 22 ± 1°C and 55 ± 10% relative humidity. Behavioural experiments
118 were conducted during the light phase. Mice that were sick or injured were excluded. Uninjured
119 cage mates were kept in the study. Performance exclusion criteria were applied to the spatial
120 object recognition task as described below. Animals were randomly assigned to experimental
121 groups and analysis was conducted blindly. Procedures complied with German animal care
122 guidelines and European Community Council Directive 86/609/EEC.

123

124 Recombinant Adeno Associated Virus (rAAV) production.

125 Viral particles were produced and purified as described previously(33) with minor
126 modifications. Specifically, AAV-293 cells (Stratagene #240073, California, USA) were used
127 for co-transfection of target AAV plasmid and helper plasmids (pFΔ6, pRV1, and pH21). Viral
128 particles in media were concentrated by incubation with 40% Polyethylene glycol (PEG)
129 solution (pH 7,4) for 3h at 4°C and centrifugation. The viral pellet was added to lysed HEK
130 cells prior to purification and concentration. For expression of shRNAs, we used a vector
131 containing the U6 promoter upstream of the shRNA sequence and a chicken β-actin promoter
132 to drive GFP expression. The sequences are as following: Dnmt3a1-shRNA1:
133 GCAGACCAACATCGAATCCAT; Dnmt3a1-shRNA2:
134 GGGAGGATGATCGAAAGGAAGGAGA; Dnmt3a2-shRNA:
135 ACGGGCAGCTATTTACAGAGC; Nrp1-shRNA1: GGAAACCAAGAAGAAATATTA; Nrp1-
136 shRNA2: GGGAGAGGAAATCGGAGCTAA; Control-shRNA: ACTACCGTTGTTATAGGTG.
137 For temporally controlled knockdown of Dnmt3a1, we used a dual-component TetON-based
138 system. The driver plasmid contained a neuron-specific promoter (hSynapsin) controlling the
139 transactivator (rtTA), the tetracycline repressor (TetR) and Kusabira Orange (KO). The second
140 construct contained GFP and a miR30-based shRNA targeting Dnmt3a1 controlled by the
141 tetracycline-responsive promoter (TRE). This vector was generated using the plasmids
142 pPRIME-CMV-GFP-FF3(34) (a gift from Stephen Elledge (Addgene plasmid # 11663;
143 http://n2t.net/addgene:11663; RRID:Addgene_11663)) and pAAV-PTRE-tight-hM3Dg-

144 mCherry(35) (a gift from William Wisden [Addgene plasmid # 66795;
145 http://n2t.net/addgene:66795; RRID:Addgene_66795]). Specifically, the Dnmt3a1-shRNA1
146 sequence was inserted into the pPRIME vector and subsequently, the GFP-miR30-Dnmt3a1-
147 shRNA expression cassette was subcloned into the vector containing the Tet-inducible
148 promoter by replacement of the hM3Dq-mCherry insert. The overexpression of Nrp1-HA or a
149 control gene, was achieved by placing HA-tagged Nrp1 or LacZ under the control of hSynapsin
150 promoter, respectively. The infection rate, toxicity, viral titer, and knockdown efficiency for
151 each batch of generated viruses were evaluated. The final titer was around 1-2 $x10^{12}$ viral
152 particles/ml.

153

154 Fluorescent labelling.

155 Sedated mice underwent intracardial perfusion with ice-cold PBS followed by 4%
156 paraformaldehyde (PFA, Sigma-Aldrich, Munich, Germany). Brains were post-fixed overnight
157 with 4% PFA solution at 4°C and subsequently transferred to 30% sucrose (in PBS). 30 µm
158 slices were cut using a cryotome (CM1950, Leica), and incubated in Hoechst 33258 (2 µg/ml,
159 Serva, Heidelberg, Germany) for 5 min. Slices were imaged using a 20x oil objective on a TCS
160 SP8 confocal microscope (Leica Microsystems, Oberkochen, Germany).

161

162 Stereotaxic surgery.

163 rAAVs were injected into the dorsal hippocampus (dHPC) at the following coordinates relative
164 to the bregma: -2 mm anteroposterior, ± 1.5 mm mediolateral, -1.7, -1.9, and -2.1 mm
165 dorsoventral from bregma. Each spot received 500 nl of viral solution injected at a speed of
166 200 nl/min through a 33G needle. After injections at each site, the needle was left in place for
167 60 s. During behavioural experiments, the experimenter was blinded to the virus injected into
168 each mouse. Behavioural testing commenced 3 weeks after rAAV delivery.

169

170 Behavioural testing.

171 Before behavioural testing, mice were habituated to the experimenter and behavioural room
172 by handling for 3 consecutive days, 1 min/mouse. Different mouse cohorts were used for
173 testing short-term (1h) or long-term memory (24h). The spatial object recognition (SOR) test
174 and contextual fear conditioning (CFC) were performed as previously described(3). In SOR,
175 mice were habituated (6 min) to an arena (50 cm × 50 cm × 50 cm) with a visual cue placed
176 on the arena wall, followed by a training session that consisted of three 6 min-exposures (3
177 min intertrial interval) to two objects. In the testing session (1h or 24h later) one object was
178 moved to a new location and object exploration was scored for 6 min. If in one experimental
179 batch during the SOR test control animals did not show a preference, due to day effects, the
180 whole set of animals was excluded from this analysis but was still included in contextual fear
181 conditioning data. Further, an animal was excluded if total exploration time during testing was
182 inferior to 2 seconds. One week later, CFC was performed in which mice were allowed to
183 explore the conditioning chamber (23 × 23 × 35 cm, TSE, Bad Homburg, Germany) for 148 s
184 followed by a 2 s foot shock (0.5 mA). They remained 30 s in the conditioning chamber before
185 returning to their home cage (HC). During testing, mice were exposed 5 mins to the
186 conditioning chamber. Where applicable, mice received intraperitoneal doxycycline hyclate
187 (2.5 mg in 500 µL saline solution, 100mg/kg, Sigma-Aldrich, Munich, Germany) 3 days prior
188 to CFC.

189 The accelerating rotarod and cued fear conditioning were performed in an independent animal
190 cohort. The rotarod apparatus (Ugo Basile, Italy) had a 3-cm diameter rod with speed
191 increasing from 4 to 40 r.p.m. over 5 min. Testing occurred 3 times daily with 1-hour intervals
192 over 3 days. Trials began at the same time of the day and ended either with mice falling off or
193 after 300 s. In cued fear conditioning, mice were put into a chamber (23 × 23 × 35 cm, TSE,
194 Germany). A white noise cue (75dB) played from 2 to 2.5 minutes after placement, followed
195 by a 0.7 mA foot shock in the last 2 seconds of the cue. Mice stayed in the chamber for an
196 extra 30 seconds before returning to their cage. During testing, mice experienced a new

197 context for 6 minutes (different chamber, smooth flat floor, altered dimensions, and a novel
198 odor). The cue started 3 minutes after placing the mice in the chamber and lasted for 3
199 minutes.

200

201 Primary hippocampal cultures and pharmacological treatments.

202 Hippocampal cultures from newborn C57Bl/6N mice (Charles River, Sulzfeld, Germany) were
203 prepared and maintained as previously described(3). In brief, mice hippocampi were
204 dissociated at P0 by papain digestion and plated onto tissue culture dishes coated with poly-
205 D-lysine and laminin (Sigma-Aldrich, Munich, Germany). The primary cultures were
206 maintained for 8 days in Neurobasal-A medium (Gibco™) supplemented with 1% rat serum
207 (Biowest), 0.5 mM L-glutamine (Sigma-Aldrich, Munich, Germany) and B27 (Gibco™),
208 followed by incubation in transfection media: salt-glucose-glycine solution (10 mM HEPES, pH
209 7.4, 114 mM NaCl, 26.1 mM NaHCO3, 5.3 mM KCl, 1 mM MgCl2, 2 mM CaCl2, 30 mM
210 glucose, 1 mM glycine, 0.5 mM C3H3NaO3, and 0.001% phenol red) and phosphate-free
211 Eagle's minimum essential medium (9:1 v/v), supplemented with insulin (7.5 µg/ml), transferrin
212 (7.5 µg/ml), and sodium selenite (7.5 ng/ml) (ITS Liquid Media Supplement, Sigma-Aldrich,
213 Munich, Germany) and penicillin-streptomycin. rAAV infection occurred on day in vitro (DIV)
214 4. Experiments were performed on DIV 9-11. To induce action potential bursting, cultures were
215 treated with 50 µM bicuculline (Alexis Biochemicals, Farmingdale, NY, USA). DNA transfection
216 was performed on DIV 8 using Invitrogen Lipofectamine 2000 (Invitrogen, CA, USA). The DNA
217 (µg): Lipofectamine (µl) ratio was 1.6:5 in 1 ml of medium. The Lipofectamine/DNA mixture
218 was left on the cells for 3 h before it was replaced with a transfection medium. Doxycycline
219 hyclate (25 µM, Sigma-Aldrich, Munich, Germany) was introduced in the medium at DIV 8. To
220 monitor doxycycline dependency, images of infected primary neurons with the TetOn-based
221 miR30 system were acquired (Axio Vert.A1, Zeiss, Oberkochen, Germany).

222

223 qRT-PCR primer design.

224 The quantitative reverse-transcription PCR (qRT-PCR) primers were designed with Primer3
225 (https://primer3.ut.ee/) using either the RefSeq curated annotation or the GENCODE VM23
226 comprehensive transcript annotation, along with the GRCm38/mm10 mouse genome
227 assembly. The specificity and amplicon product size of the primers were verified by BLAST
228 search and *in silico* PCR (UCSC Genome Browser, mm10). Primer pair efficiencies and
229 product melting curves were validated by qRT-PCR on serially diluted complementary DNA
230 (cDNA) from primary mouse hippocampal cultures (refer to the "qRT-PCR" section). The list
231 of all primers used in the study is provided in Sup Table 1.

232

233 qRT-PCR.

234 RNA from hippocampal cultures or tissue was extracted using the RNeasy Plus Mini Kit
235 (Qiagen, Hilden, Germany) with extra DNase I digestion on the column, following the
236 manufacturer's instructions. For extraction from mouse tissue, the infected region (identified
237 by GFP expression) was quickly dissected. RNA was transcribed into cDNA using the High-
238 Capacity cDNA reverse-transcription kit (Applied Biosystems, Foster City, CA, USA). qRT-
239 PCR was performed on Step One Plus Real-Time PCR System (Applied Biosystems, Foster
240 City, CA, USA) using TaqMan gene expression assays (Applied Biosystems, Foster City, CA,
241 USA) or the Power SYBR Green PCR Master Mix (Applied Biosystems) assays. The following
242 TaqMan gene expression assays were used: Dnmt1 (Mm00599763_m1), Dnmt3a1
243 (Mm00432870_m1), Dnmt3a2 (Mm00463987_m1), Dnmt3b (Mm00599800_m1) and the
244 housekeeping gene Gusb (Mm00446953_m1). Power SYBR Green PCR Master mix was
245 used for the remaining target genes. PCR reactions were run as technical triplicates in 10 µL
246 reactions (96-well format) using 0.5 µM of each primer. 2 µL of diluted cDNA (about 1.25 ng)
247 was added to each reaction. The thermal cycling was conducted with the following settings: a
248 10-minute incubation at 95 °C, 40 cycles of 10 seconds each at 95 °C, 60 °C, and 72 °C,
249 followed by a 15-second incubation at 95 °C. Melt curves were generated by heating from 60

250 °C to 90 °C at a ramp rate of 0.6 °C/min. Relative expression levels of each target transcript
251 were determined by the ΔΔCt method using beta-Actin mRNA levels as a reference(36).

252

253 Western Blotting.

254 Primary hippocampal neurons infected on DIV 4 were lysed on DIV 10 in boiling SDS sample
255 buffer (160 mM Tris-HCl (pH 6.8), 4% SDS, 30% glycerol, 10 mM dithiothreitol, and 0.02%
256 bromophenol blue). In the case of western blotting of tissue samples, dHPC was quickly
257 dissected in ice-cold PBS and homogenized in RIPA buffer (150 mM NaCl, 1% Triton X-100,
258 0.5% sodium deoxycholate, 0.1% SDS, 50 mM Tris, pH 8.0) supplemented with 1% protease
259 inhibitor cocktail (Sigma-Aldrich, Munich, Germany). Protein concentration was measured by
260 Bradford assay and 20 µg of denatured protein (in Laemmli buffer at 95°C for 5 min) was
261 loaded in a 7.5% polyacrylamide gel and blotted onto a nitrocellulose membrane (GE
262 Healthcare, Buckinghamshire, UK). The membranes were blocked in 5% milk in PBS with
263 0.01% Tween (PBST) and probed with the following antibodies (diluted in 5% milk in PBST)
264 overnight at 4 °C: α-Tubulin (1:400000, Sigma t9026), α-Dnmt3a (1:5000, H-295, Santa Cruz,
265 SC-20703), α-HA-tag (1:7500, Covance, MMS101R). The next day, membranes were
266 incubated with horseradish peroxidase-conjugated secondary antibodies (1:5000 diluted in
267 5% milk in PBST) for 1h at room temperature. Finally, they were analysed using ChemiDoc™
268 Imaging System (Bio-Rad, California, USA).

269

270 Immunocytochemistry.

271 Primary hippocampal neurons plated on coverslips were rinsed with PBS and fixed with a
272 prewarmed solution of 4% PFA and 4% sucrose for 15 min at room temperature. After
273 permeabilizing the cells in ice-cold methanol for 6 min, blocking was performed with 10%
274 normal goat serum in PBS for 1 h at room temperature. Next, cells were incubated with primary
275 antibody α-Dnmt3a (1:500, H-295, Santa Cruz, SC-20703diluted in PBS containing 2% BSA,

276 0,1% Triton X-100) overnight at 4 °C, which continued with secondary antibody incubation
277 (1:500 goat anti-mouse Alexa488 [Life Technologies, Eugene, OR, USA]) diluted in PBS
278 containing 2% BSA, 0,1% Triton X-100) for 1 h at room temperature. Finally, coverslips were
279 treated with Hoechst 33258 (2 µg/ml, Serva, Heidelberg, Germany) for 5 min and mounted on
280 glass slides. Images were acquired with a 40x oil objective on a fluorescence microscope
281 (Leica Microsystems, Oberkochen, Germany).

282

283 Bulk RNA Sequencing.

284 Total RNA from mouse hippocampal cultures was isolated as above described and 500 ng of
285 total RNA was used for bulk RNA-sequencing. Libraries were sequenced as 100bp paired-
286 end reads, amounting to approximately 61 million reads per sample. Data processing was
287 performed with R (version 3.6.3) and bioconductor (version 3.9) in Rstudio (version 1.1.463).
288 Quality control of clean sequencing reads was performed using FastQC (Babraham
289 Bioinformatics). Low-quality reads were removed using trim_galore (version 0.6.4). The
290 resulting reads were aligned to the mouse genome version GRCm38.p6 and counted using
291 kallisto version 0.46.1 (37). The count data were transformed to log2-counts per million
292 (logCPM) using the voom-function from the limma package(38). Differential expression
293 analysis was performed using the limma package in R. A false positive rate of α= 0.05 with
294 FDR correction was taken as the level of significance. Volcano plots and heatmaps were
295 created using ggplot2 package (version 2.2.1) and the complexHeatmap package (version
296 2.0.0)(39). For enrichment analysis, we used the fgsea(40), the enrichmentbrowser(41), and
297 the Enrichr packages(42).

298

299 Statistical analysis.

300 Each data set was subjected to a normality test prior to further comparisons (Shapiro-Wilk
301 normality test; alpha = 0.05). For normally distributed data sets, a two-tailed unpaired

302 Student's t-test was performed to compare two groups. If more than two groups were analyzed
303 simultaneously, a one-way ANOVA was used followed by appropriate multiple comparison
304 *post hoc* tests to control for multiple comparisons as specified. In case of a non-Gaussian
305 distribution, two-tailed Mann-Whitney tests were used to compare two distinct groups, or a
306 Kruskal-Wallis test followed by Dunn´s *post hoc* test to compare more than two groups. The
307 sample size was determined based on similar experiments carried out in the past and the
308 literature. All plotted data represent mean ± SEM. Statistical analysis was performed using
309 GraphPad Prism 7 (GraphPad Software). All behavioural sessions were video recorded and
310 manually scored to determine the exploration of objects during training and testing phases or
311 freezing behaviour by an experimenter blind to the group identity. The TSE Systems Fear
312 Conditioning program was used to score the mean velocity during the training for CFC.

313

314

315 **Results**

316

317 **Dnmt3a1 is required for long-term memory formation**

318 In this study, we sought to investigate the role of DNA methyltransferase 3a1 (Dnmt3a1) in
319 neuronal function and memory formation. We employed stereotaxic surgery and recombinant
320 adeno-associated viruses (rAAVs) to deliver a control shRNA sequence (Control-shRNA)(3)
321 or two independent shRNAs to knockdown Dnmt3a1 into the adult (8 weeks) dorsal
322 hippocampus (dHPC) of mice (Figure 1A, B). We used the rAAV1/2 serotype given its well
323 established neuronal tropism(43). To monitor viral expression upon infection, the viral
324 constructs contained a GFP cassette under the control of the chicken-beta-actin promoter
325 (Figure 1A, B). We confirmed knockdown efficiency of our shRNAs by transfection of primary
326 hippocampal neurons *in vitro* and immunostaining against endogenous Dnmt3a1 (Sup Figure
327 1A). To further validate the knockdown efficiency *in vivo*, we performed qRT-PCR and western
328 blot analysis of dHPC of mice infected with the viral constructs (Sup Figure 1B-G). We

329 confirmed that both sequences selectively knockdown Dnmt3a1 without affecting other *Dnmts*.
330 shRNA1 and shRNA2 sequences effectively reduced Dnmt3a1 expression at both the mRNA
331 (Sup Figure 1B; two-tailed, unpaired t-test; *Dnmt3a1*: $t_{(6)}$=6.28; *Dnmt3a2*: $t_{(6)}$=0.48; *Dnmt1*:
332 $t_{(6)}$=0.81; *Dnmt3b*: $t_{(6)}$=0.09; C; two-tailed, unpaired t-test; *Dnmt3a1*: $t_{(8)}$=5.94; *Dnmt3a2*:
333 $t_{(7)}$=1.07; *Dnmt1*: $t_{(8)}$=0.52; *Dnmt3b*: $t_{(8)}$=1.17;) and protein (Sup Figure 1D-G; two-tailed,
334 unpaired t-test; Dnmt3a1-shRNA1: $t_{(6)}$=6.15; Dnmt3a1-shRNA2: $t_{(7)}$=3.16) levels. To evaluate
335 a requirement for Dnmt3a1 in memory performance, we conducted hippocampus-dependent
336 memory tests on mice three weeks after stereotaxic surgery (Figure 1C). We found that, when
337 tested 24 hours after training in the spatial object recognition test, mice injected with either
338 Dnmt3a1-shRNA1 or -shRNA2 exhibited no preference for the displaced object (Figure 1D;
339 two-tailed, unpaired t-test; Dnmt3a1-shRNA1: $t_{(17)}$=2.43; Dnmt3a1-shRNA2: $t_{(22)}$=3.15).
340 However, when evaluated 1 hour after training, mice in shRNA groups explored the displaced
341 object for a length of time comparable to the control group (Figure 1E; two-tailed, unpaired t-
342 test; Dnmt3a1-shRNA1: $t_{(10)}$=2.04; Dnmt3a1-shRNA2: $t_{(18)}$=0.64). Importantly, Dnmt3a1
343 knockdown did not affect the overall amount of time that mice spent exploring the objects
344 during training (Sup Figure 1H, I; two-tailed, unpaired t-test; Dnmt3a1-shRNA1: $t_{(17)}$=0.92;
345 Dnmt3a1-shRNA2: $t_{(22)}$=0.35). To assess further the role of hippocampal Dnmt3a1 in memory
346 formation, we trained mice in contextual fear conditioning. Knockdown of Dnmt3a1 with either
347 shRNA1 or shRNA2 impaired contextual fear memory response 24 hours after training (Figure
348 1F; two-tailed, unpaired t-test; Dnmt3a1-shRNA1: $t_{(20)}$=2.60; Dnmt3a1-shRNA2: $t_{(20)}$=2.54)
349 without decreasing freezing levels compared to the Control-shRNA when tested 1 hour after
350 training (Figure 1G; two-tailed, unpaired t-test; Dnmt3a1-shRNA1: $t_{(15)}$=0.04; Dnmt3a1-
351 shRNA2: $t_{(22)}$=0.90). This decrease in freezing was not due to altered responsiveness to the
352 shock administration during the training session (Sup Figure 1 J, K; two-tailed, unpaired t-test;
353 Dnmt3a1-shRNA1; Pre-Shock: $t_{(20)}$=0.16; Shock: $t_{(20)}$=0.25; Dnmt3a1-shRNA2: Pre-Shock:
354 $t_{(21)}$=1.06; Shock: $t_{(21)}$=0.36). These results show that Dnmt3a1 knockdown impairs long-term
355 memory formation without affecting short-term memory. Next, we investigated whether the
356 memory deficits are specific to hippocampus-dependent tasks. We assessed the performance

357 of mice injected with Control-shRNA, Dnmt3a1-shRNA-1 or Dnmt3a1-shRNA-2 in the auditory
358 cue fear conditioning (Sup Figure 1L) and accelerating rotarod (Sup Figure 1M), two tasks
359 that do not require hippocampal function(44,45). We found that hippocampal Dnmt3a1
360 knockdown did not affect cued long-term fear memory (Sup Figure 1L; one-way ANOVA test
361 followed by Dunnett's multiple comparisons test; $F_{(2,32)}$=0.18, p=0.84) or motor skill learning
362 (Sup Figure 1M; two-way repeated measures ANOVA; effect of training day $F_{(1.661,53.15)}$=11.76;
363 effect of virus $F_{(2,32)}$=0.51), indicating region-specific deficits.

364 The behavioural testing in this series of experiments was carried out three weeks following
365 stereotaxic delivery of rAAVs to achieve high viral expression and, as a result, high knockdown
366 efficiency. However, the persistent reduction of Dnmt3a1 levels may lead to network-wide
367 changes that could impact learning and memory. Consequently, in order to more directly
368 assign a role for Dnmt3a1 in mature neurons during the process of memory formation, we
369 adopted a temporally controlled method that limited Dnmt3a1 knockdown to the time of
370 behavioural testing. We used a TetON-based system that consisted of two components: for
371 tight control of Tet-dependent transgene expression in neurons, one viral construct contained
372 the human synapsin (hSyn) promoter controlling the expression of the reverse tetracycline-
373 controlled transactivator (rtTA) together with the Tet repressor (TetR) and the fluorescent
374 protein Kusabira Orange (KO) that serves as an infection marker(46,47). In the second
375 construct, the Dnmt3a1-specific shRNA sequence 1 or the Control-shRNA was embedded in
376 a microRNA-30-based expression cassette(34), which is under the control of the tetracycline
377 responsive promoter (TRE) (Figure 2A-B). In the absence of doxycycline, TetR is bound to
378 TRE inhibiting its activity. Upon doxycycline administration, TetR releases from the TRE
379 promoter allowing the binding of the activator rtTA. Administration of doxycycline to
380 hippocampal primary cultures verified tight control of transgene expression via the Tet-On
381 system (Sup Figure 2 A-D). The expression of GFP after doxycycline administration increased
382 over a time course of 72 hours (Sup Figure 2B). Western blot analysis of Dnmt3a1 at the same
383 time points revealed a significant knockdown of Dnmt3a1 protein levels at 72 hours (Sup

384 Figure 2C, D; two-tailed, unpaired t-test; 0h: $t_{(10)}$=1.03; 48h: $t_{(10)}$=1.86; 72h: $t_{(10)}$=3.06; Mann-
385 Whitney test; 24h: U=10). Thus, doxycycline was injected intraperitoneally 72 hours before
386 behavioural testing (Figure 2C). We found that knocking down hippocampal Dnmt3a1 around
387 the time of fear conditioning reduced freezing levels when mice were tested 24 hours after
388 training (Figure 2D; two-tailed, unpaired t-test: $t_{(27)}$=2.99); however, mice froze to a similar
389 extent than the control mice when testing occurred 1 hour after training (Figure 2E; two-tailed,
390 unpaired t-test: $t_{(18)}$=0.32). The responsiveness to the shock administration during the training
391 session did not cause this decrease in freezing (Sup Figure 2E; two-tailed, unpaired t-test;
392 Pre-Shock: $t_{(14)}$=0.47; Shock: $t_{(14)}$=0.80). Taken together, these findings further support a
393 function of Dnmt3a1 during long-term memory formation and suggest that Dnmt3a1
394 participates in the regulation of learning-dependent gene expression required for long-term
395 memory.

396

397 **Dnmt3a1 regulates the expression of activity-dependent genes involved in synaptic**
398 **plasticity**

399 Next, to elucidate the molecular mechanism by which Dnmt3a1 regulates memory
400 consolidation we sought to identify activity-dependent genes regulated by Dnmt3a1. To this
401 end, we performed RNA sequencing of hippocampal neurons infected with Dnmt3a1-shRNA2
402 or a Control-shRNA after inducing neuronal activity by bicuculline treatment (Figure 3A, B,
403 Sup Figure 3A, B). In control conditions, we found that neuronal activity leads to the
404 downregulation of 1981 genes and upregulation of 1935 genes including established activity-
405 regulated genes, e.g., Arc, Fos, Npas4 (Figure 3C, Sup File 1).

406 To identify genes dependent on Dnmt3a1, we focused on genes that are differentially
407 expressed in Dnmt3a1 knockdown versus control conditions in basal (Figure 3D, Sup File 2)
408 and/or upon bicuculline treatment (Figure 3D, Sup File 2). Notably, the expression of classical
409 immediate early genes, such as Arc, Fos, Npas4 was not altered in Dnmt3a1-shRNA
410 conditions (Figure 3D, Sup File 2), suggesting that the identified changes are not a result of

411 an overall disruption of neuronal responses. We hypothesised that Dnmt3a1-regulated genes
412 that are involved in memory formation should be a) differentially expressed in response to
413 Dnmt3a1 reduction and b) activity-regulated. Thus, we overlapped the activity-regulated
414 (Figure 3C, Sup File 1) and the Dnmt3a1-regulated gene sets (Figure 3D, Sup File 2) in order
415 to find potential activity-regulated Dnmt3a1 target genes. This intersection identified 491
416 candidates (Sup Figure 3B,C, Sup File 3). Gene ontology (GO) analysis of the 491 genes
417 yielded a strong enrichment for terms related to structural and functional plasticity, namely
418 *"Neuropeptide signaling pathway"*, *"Regulation of signaling receptor activity"* and *"Regulation*
419 *of cell-substrate adhesion"* (Figure 3E, Sup File 3). This suggests that genes downstream of
420 Dnmt3a1 may play an important role in synaptic plasticity and learning and memory. We
421 confirmed some of the identified Dnmt3a1 target genes in independent biological samples
422 using qRT-PCR (Figure 3F, G). To further rule out the possibility of off-target effects, this
423 validation was performed using the two independent shRNA sequences. We confirmed that
424 the expression of *Alkal2*, *Cacng5*, *Nrp1, Crhbp, Npy and Trpc6* is activity-regulated (Figure
425 3F,G; one-way ANOVA test followed by Sidak's multiple comparisons test: *Alkal2*:
426 $F_{(6,56)}=78.46$, $p<0.0001$; *Cacng5*: $F_{(6,56)}=16.67$, $p<0.001$; *Nrp1*: $F_{(6,49)}=46.53$, $p<0.0001$; *Crhbp*:
427 $F_{(6,42)}=13.60$, $p<0.0001$; *Npy*: $F_{(6,56)}=15.66$, $p<0.001$; *Trpc6*: $F_{(6,49)}=5.373$, $p=0.003$). The
428 expression of the Control-shRNA sequence appeared to cause a mild effect on the expression
429 of Nrp1, but not of the other genes (comparison to uninfected control). However, this was not
430 replicated across independent experiments (see Sup Figure 3F). Furthermore, we found that
431 the expression of *Alkal2*, *Cacng5*, and *Nrp1* is reduced upon Dnmt3a1 depletion achieved by
432 shRNA1 or shRNA2 (Figure 3F), whereas *Crhbp, Npy and Trpc6* failed to show a significant
433 effect with one of the shRNA sequences (Figure 3G).

434 *Dnmt3a* encodes for two distinct isoforms Dnmt3a1 and Dnmt3a2, which are differentially
435 regulated by neuronal activity(22,23). We further investigated whether the two isoforms
436 regulate distinct targets. To test this, we infected primary hippocampal cultures with a
437 previously validated shRNA to reduce Dnmt3a2 levels(23,24) (Sup Figure 3D) and

438 investigated the impact of this manipulation on the expression of the identified Dnmt3a1-
439 regulated genes. Reduction of Dnmt3a2 did not change the expression of *Alkal2*, *Cacng5* or
440 *Nrp1* neither in basal conditions nor upon neuronal activity (Sup Figure 3E; one-way ANOVA
441 test followed by Sidak's multiple comparisons test: *Alkal2*: $F_{(5,25)}$=49.04, p<0.0001; *Cacng5*:
442 $F_{((5,25)}$=4.96, p=0.0044; *Nrp1*: $F_{(4,25)}$= 4.96, p=0.0044). Taken together these findings
443 demonstrate that Dnmt3a1 is required for the regulation of a synaptic plasticity-related
444 transcriptional program and further suggest that the Dnmt3a2 isoform may regulate a distinct
445 gene pool.

446

447 **Neuropilin-1 is a Dnmt3a1 downstream target required for memory formation**

448 Next, we aimed at investigating whether Dnmt3a1 role in memory consolidation requires the
449 activity of identified target genes. Among the genes whose expression is controlled by
450 Dnmt3a1, we focused on neuronal genes which have been identified to be regulated by novel
451 environment exposure in the mouse hippocampus(48). These included, among others, the
452 previously validated gene Neuropilin-1 (*Nrp1)* (Figure 3G, H). Nrp1 is known to build a complex
453 with Semaphorin 3a (Sema3A) and Plexin A4 and is implicated in signalling pathways
454 regulating neuronal morphology(31,49). Although it has been demonstrated that this complex
455 is important for AMPA receptor trafficking(50), is still unknown whether Nrp1 plays a role in
456 hippocampus-dependent memory formation. We performed a shRNA-mediated loss-of-
457 function approach to assess the role of Nrp1 in memory formation. We generated two
458 independent shRNA constructs to reduce the expression of *Nrp1* (Figure 4A) and validated
459 their knockdown efficiency *in vivo* after stereotaxic delivery of the viral constructs or a Control-
460 shRNA into the dHPC. We confirmed that Nrp1-shRNA1 and -shRNA2 sequences led to a
461 robust reduction of Nrp1 mRNA levels (Sup Figure 4A, B; two-tailed, unpaired t-test: Nrp1-
462 shRNA1: $t_{(10)}$=5.28; Nrp1-shRNA2: $t_{(16)}$=7.25). Mice were subjected to a hippocampus-
463 dependent behavioural memory task three weeks after viral delivery (Figure 4B). Knockdown
464 of Nrp1 with either shRNA resulted in exploration of the displaced object at chance levels

465 (Figure 4C; one-way ANOVA test followed by Dunnett's multiple comparisons test: $F_{(2,29)}$=4.46,
466 p=0.0204), as well as in decreased freezing responses in the contextual fear conditioning test
467 compared to mice injected with the Control-shRNA (Figure 4D; one-way ANOVA test followed
468 by Dunnett's multiple comparisons test: $F_{(2,30)}$=6.13, p=0.0059). Notably, Nrp1 knockdown did
469 not affect the overall object exploration time (Sup Figure 4C; one-way ANOVA test followed
470 by Dunnett's multiple comparisons test: $F_{(2,32)}$=0.80, p=0.4584) or the responsiveness to the
471 shock administration (Sup Figure 4D; one-way ANOVA test followed by Sidak's multiple
472 comparisons test: $F_{(5,62)}$=83.97, p<0.0001). In conclusion, this set of experiments uncovered a
473 novel function for Nrp1 in long-term memory formation.

474

475 **Dnmt3a1, but not Dnmt3a2, regulates long-term memory formation via its downstream**
476 **target Nrp1**

477 To evaluate a function of Nrp1 as a downstream effector of Dnmt3a1 during memory
478 formation, we performed a rescue experiment. To this end, we overexpressed HA-tagged
479 Nrp1 or a control protein (LacZ) under the regulation of hSyn promoter together with either
480 Dnmt3a1-shRNA2 or Control-shRNA sequences in the mouse hippocampus (Figure 5A, B).
481 We first confirmed successful overexpression of Nrp1 in the dHPC by western blot analysis
482 (Sup Figure 5A, B). After stereotaxic delivery of the constructs, mice underwent the spatial
483 object recognition task (Figure 5B). The different groups did not exhibit differences in the time
484 spent exploring the objects during the training session (Sup Figure 5C; one-way ANOVA test
485 followed by Dunnett's multiple comparisons test: $F_{(3,48)}$=0.12, p=0.9477). As shown above, the
486 reduction of Dnmt3a1 levels caused memory impairments which are manifested by the
487 decreased preference for the displaced object (Figure 1D). Strikingly, this impairment was
488 rescued upon Nrp1 overexpression (Figure 5C; one-way ANOVA test followed by Sidak's
489 multiple comparisons test: $F_{(3,46)}$=7.39, p=0.004). Mice that overexpressed Nrp1 and
490 expressed a control shRNA sequence showed memory performance similar to the control
491 group (Figure 5C). Taken together, these results demonstrate that Nrp1 acts downstream of

492 Dnmt3a1, is required for memory formation and can per se rescue Dnmt3a1-dependent
493 memory impairments. Thus, indicating that Dnmt3a1 regulates memory formation, at least in
494 part, via its downstream target Nrp1.

495 Our gene expression analysis suggested that the isoforms Dnmt3a1 and Dnmt3a2 regulate
496 distinct genes. Specifically, we showed that Nrp1 expression is regulated by Dnmt3a1, but it
497 is not altered upon knockdown of Dnmt3a2 (Sup Figure 3D). Next, to investigate a specific
498 functional link between Dnmt3a1, Nrp1 and memory formation, we tested if Nrp1
499 overexpression rescues Dnmt3a2-knockdown-dependent memory impairments. We
500 overexpressed HA-tagged Nrp1 with a Dnmt3a2-specific shRNA sequence in the mouse
501 dorsal hippocampus and performed the spatial object recognition task in mice (Figure 5D, E).
502 Importantly, none of the conditions showed differences in overall time exploring the objects
503 during training (Sup Figure 5D; one-way ANOVA test followed by Sidak's multiple
504 comparisons test: $F_{(2,32)}=1.92$, $p=0.1633$). As previously described(23), knockdown of
505 Dnmt3a2 impaired spatial object recognition memory and remarkably, this impairment was not
506 rescued upon Nrp1 overexpression (Figure 5F; one-way ANOVA test followed by Sidak's
507 multiple comparisons test: $F_{(2,32)}=10$, $p=0.0002$). This finding shows that the rescue obtained
508 in response to Nrp1 overexpression is not a result of a generalized memory enhancement
509 effect and further supports that Nrp1 acts downstream of Dnmt3a1 but not Dnmt3a2. Thus,
510 this data uncovers a *Dnmt3a* isoform specific mechanism in memory formation.

511

512

513

514 **Discussion**

515

516 In this study we demonstrated a critical role for Dnmt3a1 in long-term memory formation by
517 showing that acute knockdown of Dnmt3a1 in the adult hippocampus selectively impairs long-
518 term memory formation and further identified activity-dependent genes regulated by Dnmt3a1

levels. Furthermore, our data suggests that despite a requirement for both Dnmt3a1 and Dnmt3a2 for memory formation, the two isoforms regulate this process via distinct mechanisms; Nrp1 overexpression rescued Dnmt3a1, but not Dnmt3a2, knockdown-driven impairments in memory formation. Taken together these findings have advanced our understanding of the requirement for distinct Dnmts in mnemonic processes as well as of the identity of downstream effector molecules.

Most studies that aimed at investigating the role of Dnmt3a in adult brain cognition have utilized heterozygous constitutive(51) or conditional knock-out mice(15,16,52). These models delete *Dnmt3a* during critical prenatal and postnatal neurodevelopmental phases, which may confound the interpretation of the function of *Dnmt3a*-coded proteins in memory formation in the adult. Mitchnick and colleagues (2015) used small interfering RNAs to acutely disrupt *Dnmt3a* expression in the adult hippocampus and provided compelling evidence for a role of *Dnmt3a*-coding genes in long-term hippocampal memory formation(14). In addition, our present and previous studies(23–25) have corroborated these findings and demonstrated that both Dnmt3a isoforms, Dnmt3a1 and Dnmt3a2, are required for memory formation in adult mature neurons. This study has further identified for the first time an activity-regulated genomic program regulated by Dnmt3a1 levels in hippocampal neurons. We found that the knockdown of Dnmt3a1 altered the expression of several genes both in baseline as well as upon neuronal activation. Even if counterintuitive at first, the reduction of Dnmt expression resulted not only in de-repression of gene expression, but also downregulation. Although these gene expression changes are likely a combination of direct effects on the altered genes and indirect mechanisms via the disruption of expression of other transcriptional regulatory processes, these findings corroborate previous studies in which a link between transcription activation and DNA methylation has been shown(10,28,53). In our transcriptomic analysis we found that Dnmt3a1 regulates the expression of several genes with key roles in synaptic plasticity and memory. Namely, we found changes in the expression of *Npy*, *Cort*, *Trpc6*, which have been implicated in memory consolidation(54–56). Upon the confirmation with two

546 independent shRNA sequences, we focused on Nrp1 which has been shown to be regulated
547 by enriched environment exposure(57) and within dentate gyrus memory engrams(48).
548 Besides the established function for the semaphorins and their receptors (Nrp and plexin
549 family members) in neurodevelopment(32,58), only a few lines of evidence demonstrated their
550 involvement in homeostatic and Hebbian forms of plasticity in the adult
551 hippocampus(31,50,59,60). Notably, Nrp1 is localised at synapses of the adult rat
552 hippocampus(60) and secreted semaphorins acting on the sema-Nrp-plexin complex
553 modulate synaptic connectivity in granule cells of dentate gyrus and pyramidal neurons of
554 CA1(60) as well as AMPA receptor trafficking in CA3-CA1 synapses(50). The present study
555 adds to this body of literature by demonstrating that Nrp1 is required for the formation of
556 hippocampal long-term memory. Intriguingly, we showed that overexpression of hippocampal
557 Nrp1 rescued Dnmt3a1 knockdown-dependent memory impairments. Thus, our findings
558 suggest that the regulation of Nrp1-dependent mechanisms during memory consolidation is a
559 mechanism via which Dnmt3a1 contributes to memory formation.

560 This study uncovered a dissociation in the downstream processes regulated by the Dnmt3a
561 isoforms during hippocampal long-term memory formation. Notably, we showed that Nrp1
562 overexpression selectively rescued memory impairments promoted by the reduction of
563 Dnmt3a1, but not Dnmt3a2, levels in the adult hippocampus. Our previous work had already
564 demonstrated differential regulation of the two enzymes upon neuronal activity and learning.
565 In contrast to Dnmt3a1, Dnmt3a2 mRNA levels are induced in response to action potential
566 bursting and learning(23), cocaine administration(30) and an inflammatory response(29) in
567 different regions of the central nervous system. Despite the lack of regulation at the level of
568 transcription, Dnmt3a1 protein levels appear to be regulated upon neuronal activity(22). It has
569 also been shown that Dnmt3a isoforms target unique genomic loci(21,61). Collectively, these
570 findings indicate distinct regulatory functions. Specifically, during the formation of memory,
571 lack of redundancy is further supported by our studies that showed that impairments in long-
572 term memory formation promoted by the acute, reduced hippocampal expression of Dnmt3a1

573 or Dnmt3a2 are not compensated by the other isoform. Thus, the emerging picture is that the
574 distinct Dnmts are required for cognitive abilities through the regulation of complementary but
575 non-overlapping processes. The recruitment of Dnmts to DNA is thought to be guided by
576 chromatin marks, namely histone modifications(62) and non-coding RNA species that direct
577 gene-specific methylation patterns(63–67). Notably, differential DNA recruitment between
578 Dnmt3a1 and Dnmt3a2 may be at least in part driven by distinct recognition of histone tail
579 marks(21,28,68,69). Moreover, the N-terminus unique to Dnmt3a1 has been shown to confer
580 specific chromatin recognition properties to this isoform(28,69). Future studies should
581 elucidate the mechanisms that dictate the regulation of distinct downstream targets for
582 Dnmt3a1 and Dnmt3a2 in response to neuronal activity.

583 Our findings highlight the complex and highly regulated role of distinct epigenetic regulators
584 in brain function. The relevance of investigating DNA methylation processes in the nervous
585 system is further underscored by the multiple lines of evidence that demonstrated that DNA
586 methylation dysregulation underlies several pathological conditions, such as
587 neurodevelopmental(70) and neurodegenerative(71) diseases as well as psychiatric
588 conditions(72,73) and chronic pain(74). Therefore, the elucidation of the regulatory
589 mechanisms controlled by the various epigenetic factors is required to gain further
590 understanding of the pathophysiological mechanisms underlying these conditions.

591

592

593 **Acknowledgements**

594 We thank David V.C. Brito, Kübra Gülmez Karaca and Stefanos Loizou for their critical
595 comments on the manuscript. Celia García-Vilela, Carmen Leibold, Stefanos Loizou, and
596 Benjamin Zeuch for technical support. hSyn-LacZ construct was kindly gifted by Prof. Dr.
597 Daniela Mauceri. This work was supported by the Deutsche Forschungsgemeinschaft (DFG)
598 [grant numbers OL 437/1, OL 437/2, OL 437/3 and OL 437/4 to A.M.M.O.], the Chica and

Heinz Schaller Foundation [fellowship and research award to A.M.M.O.], and the Joachim Herz Stiftung [Add-on Fellowships for Interdisciplinary Life Science to J.Kupke.].

Author Contributions: JKupke, AMMO designed research; JKupke, JKlimmt, FM, MS, AMMO performed experiments; JKupke, JKlimmt, FM, MS, CS, AMMO, PL, CP analyzed and interpreted data; JKupke, AMMO wrote the paper. All authors edited the manuscript.

Conflict of Interest

The authors declare no conflicts of interest.

Data availability

The RNA-Sequencing data analysed in this study is publicly available at the National Center for Biotechnology Information (NCBI) Gene Expression Omnibus (GEO) with the accession number GSE232630.

References

1. Benito E, Barco A. The Neuronal Activity-Driven Transcriptome. Mol Neurobiol. 2015 Jun 17;51(3):1071–88.
2. Yap EL, Greenberg ME. Activity-Regulated Transcription: Bridging the Gap between Neural Activity and Behavior. Vol. 100, Neuron. 2018.
3. Brito DVC, Kupke J, Karaca KG, Zeuch B, Oliveira AMM. Mimicking age-associated Gadd45γ dysregulation results in memory impairments in young adult mice. Journal of Neuroscience. 2020;40(6).
4. Alberini CM. Transcription Factors in Long-Term Memory and Synaptic Plasticity. Physiol Rev. 2009 Jan;89(1):121–45.
5. Alberini CM, Kandel ER. The Regulation of Transcription in Memory Consolidation. Cold Spring Harb Perspect Biol. 2015 Jan;7(1):a021741.
6. Cholewa-Waclaw J, Bird A, von Schimmelmann M, Schaefer A, Yu H, Song H, et al. The Role of Epigenetic Mechanisms in the Regulation of Gene Expression in the Nervous System. The Journal of Neuroscience. 2016 Nov 9;36(45):11427–34.

630 7. Day JJ, Sweatt JD. Epigenetic Mechanisms in Cognition. Neuron. 2011
631 Jun;70(5):813–29.
632 8. Oliveira AMM. DNA methylation: a permissive mark in memory formation and
633 maintenance. Learning & Memory. 2016 Oct 15;23(10):587–93.
634 9. Medrano-Fernández A, Barco A. Nuclear organization and 3D chromatin architecture
635 in cognition and neuropsychiatric disorders. Mol Brain. 2016 Dec 5;9(1):83.
636 10. Suzuki MM, Bird A. DNA methylation landscapes: provocative insights from
637 epigenomics. Nat Rev Genet. 2008 Jun;9(6):465–76.
638 11. Halder R, Hennion M, Vidal RO, Shomroni O, Rahman RU, Rajput A, et al. DNA
639 methylation changes in plasticity genes accompany the formation and maintenance of
640 memory. Nat Neurosci. 2015;19(1).
641 12. Guo JU, Ma DK, Mo H, Ball MP, Jang MH, Bonaguidi MA, et al. Neuronal activity
642 modifies the DNA methylation landscape in the adult brain. Nat Neurosci. 2011 Oct
643 28;14(10):1345–51.
644 13. Miller CA, Sweatt JD. Covalent Modification of DNA Regulates Memory Formation.
645 Neuron. 2007 Mar;53(6):857–69.
646 14. Mitchnick KA, Creighton S, O'Hara M, Kalisch BE, Winters BD. Differential
647 contributions of *de novo* and maintenance DNA methyltransferases to object memory
648 processing in the rat hippocampus and perirhinal cortex - a double dissociation.
649 European Journal of Neuroscience. 2015 Mar;41(6):773–86.
650 15. Feng J, Zhou Y, Campbell SL, Le T, Li E, Sweatt JD, et al. Dnmt1 and Dnmt3a
651 maintain DNA methylation and regulate synaptic function in adult forebrain neurons.
652 Nat Neurosci. 2010 Apr 14;13(4):423–30.
653 16. Morris MJ, Adachi M, Na ES, Monteggia LM. Selective role for DNMT3a in learning
654 and memory. Neurobiol Learn Mem. 2014 Nov;115:30–7.
655 17. Zocher S, Overall RW, Berdugo-Vega G, Rund N, Karasinsky A, Adusumilli VS, et
656 al. *De novo* DNA methylation controls neuronal maturation during adult hippocampal
657 neurogenesis. EMBO J. 2021 Sep 15;40(18).
658 18. Tatton-Brown K, Zachariou A, Loveday C, Renwick A, Mahamdallie S, Aksglaede L,
659 et al. The Tatton-Brown-Rahman Syndrome: A clinical study of 55 individuals with de
660 novo constitutive DNMT3A variants. Wellcome Open Res. 2018 Apr 23;3:46.
661 19. Tatton-Brown K, Seal S, Ruark E, Harmer J, Ramsay E, del Vecchio Duarte S, et al.
662 Mutations in the DNA methyltransferase gene DNMT3A cause an overgrowth
663 syndrome with intellectual disability. Nat Genet. 2014 Apr 9;46(4):385–8.
664 20. Chen T, Ueda Y, Xie S, Li E. A Novel Dnmt3a Isoform Produced from an Alternative
665 Promoter Localizes to Euchromatin and Its Expression Correlates with Activede Novo
666 Methylation. Journal of Biological Chemistry. 2002 Oct;277(41):38746–54.
667 21. Manzo M, Wirz J, Ambrosi C, Villaseñor R, Roschitzki B, Baubec T. Isoform-specific
668 localization of DNMT3A regulates DNA methylation fidelity at bivalent CpG islands.
669 EMBO J. 2017 Dec 26;36(23):3421–34.
670 22. Bayraktar G, Yuanxiang PA, Confettura AD, Gomes GM, Raza SA, Stork O, et al.
671 Synaptic control of DNA methylation involves activity-dependent degradation of
672 DNMT3A1 in the nucleus. Neuropsychopharmacology. 2020;45(12).
673 23. Oliveira AMM, Hemstedt TJ, Bading H. Rescue of aging-associated decline in
674 Dnmt3a2 expression restores cognitive abilities. Nat Neurosci. 2012;15(8).
675 24. Oliveira AMM, Hemstedt TJ, Freitag HE, Bading H. Dnmt3a2: A hub for enhancing
676 cognitive functions. Mol Psychiatry. 2016;21(8).
677 25. Gulmez Karaca K, Kupke J, Brito DVC, Zeuch B, Thome C, Weichenhan D, et al.
678 Neuronal ensemble-specific DNA methylation strengthens engram stability. Nat
679 Commun. 2020;11(1).

26. Feng J, Chang H, Li E, Fan G. Dynamic expression of de novo DNA methyltransferases Dnmt3a and Dnmt3b in the central nervous system. J Neurosci Res. 2005 Mar 15;79(6):734–46.
27. Guo JU, Szulwach KE, Su Y, Li Y, Yao B, Xu Z, et al. Genome-wide antagonism between 5-hydroxymethylcytosine and DNA methylation in the adult mouse brain. Front Biol (Beijing). 2014 Feb 6;9(1):66–74.
28. Gu T, Hao D, Woo J, Huang TW, Guo L, Lin X, et al. The disordered N-terminal domain of DNMT3A recognizes H2AK119ub and is required for postnatal development. Nat Genet. 2022 May 9;54(5):625–36.
29. Oliveira AM, Litke C, Paldy E, Hagenston AM, Lu J, Kuner R, et al. Epigenetic control of hypersensitivity in chronic inflammatory pain by the de novo DNA methyltransferase Dnmt3a2. Mol Pain. 2019 Jan 4;15:174480691982746.
30. Cannella N, Oliveira AMM, Hemstedt T, Lissek T, Buechler E, Bading H, et al. Dnmt3a2 in the Nucleus Accumbens Shell Is Required for Reinstatement of Cocaine Seeking. The Journal of Neuroscience. 2018 Aug 22;38(34):7516–28.
31. Carulli D, de Winter F, Verhaagen J. Semaphorins in Adult Nervous System Plasticity and Disease. Vol. 13, Frontiers in Synaptic Neuroscience. 2021.
32. Pasterkamp RJ. Getting neural circuits into shape with semaphorins. Nat Rev Neurosci. 2012 Sep 16;13(9):605–18.
33. Gulmez Karaca K, Brito DVC, Kupke J, Zeuch B, Oliveira AMM. Engram reactivation during memory retrieval predicts long-term memory performance in aged mice. Neurobiol Aging. 2021 May;101:256–61.
34. Stegmeier F, Hu G, Rickles RJ, Hannon GJ, Elledge SJ. A lentiviral microRNA-based system for single-copy polymerase II-regulated RNA interference in mammalian cells. Proc Natl Acad Sci U S A. 2005;102(37).
35. Zhang Z, Ferretti V, Güntan I, Moro A, Steinberg EA, Ye Z, et al. Neuronal ensembles sufficient for recovery sleep and the sedative actions of α 2 adrenergic agonists. Nat Neurosci. 2015;18(4).
36. Brito DVC, Gulmez Karaca K, Kupke J, Frank L, Oliveira AMM. MeCP2 gates spatial learning-induced alternative splicing events in the mouse hippocampus. Mol Brain. 2020 Dec 17;13(1):156.
37. Bray NL, Pimentel H, Melsted P, Pachter L. Near-optimal probabilistic RNA-seq quantification. Nat Biotechnol. 2016;34(5).
38. Ritchie ME, Phipson B, Wu D, Hu Y, Law CW, Shi W, et al. Limma powers differential expression analyses for RNA-sequencing and microarray studies. Nucleic Acids Res. 2015;43(7).
39. Gu Z, Eils R, Schlesner M. Complex heatmaps reveal patterns and correlations in multidimensional genomic data. Bioinformatics. 2016;32(18).
40. Korotkevich G, Sukhov V, Budin N, Shpak B, Artyomov MN, Sergushichev A. Fast gene set enrichment analysis. bioRxiv [Internet]. 2021 Jan 1;060012. Available from: http://biorxiv.org/content/early/2021/02/01/060012.abstract
41. Geistlinger L, Csaba G, Zimmer R. Bioconductor's EnrichmentBrowser: seamless navigation through combined results of set- & network-based enrichment analysis. BMC Bioinformatics. 2016 Dec 20;17(1):45.
42. Chen EY, Tan CM, Kou Y, Duan Q, Wang Z, Meirelles G V, et al. Enrichr: Interactive and collaborative HTML5 gene list enrichment analysis tool. BMC Bioinformatics. 2013;14.
43. Xu R, Janson CG, Mastakov M, Lawlor P, Young D, Mouravlev A, et al. Quantitative comparison of expression with adeno-associated virus (AAV-2) brain-specific gene cassettes. Gene Ther. 2001;8(17).

44. Hikosaka O, Nakamura K, Sakai K, Nakahara H. Central mechanisms of motor skill learning. Curr Opin Neurobiol. 2002 Apr;12(2):217–22.
45. Maren S. Neurobiology of Pavlovian Fear Conditioning. Annu Rev Neurosci. 2001 Mar;24(1):897–931.
46. Terzi F, Knabbe J, Cambridge SB. In Vivo Optical Interrogation of Neuronal Responses to Genetic, Cell Type-Specific Silencing. J Neurosci [Internet]. 2023 Dec 13 [cited 2024 Jan 6];43(50):JN-RM-2253-22. Available from: https://pubmed.ncbi.nlm.nih.gov/37923378/
47. Brito DV, Kupke J, Sokolov R, Sidney Cambridge P, Martin Both P, Peter Bengtson C, et al. Biphasic Npas4 expression promotes inhibitory plasticity and suppression of fear memory consolidation in mice. [cited 2024 Jan 6]; Available from: https://doi.org/10.1101/2023.11.17.567527
48. Jaeger BN, Linker SB, Parylak SL, Barron JJ, Gallina IS, Saavedra CD, et al. A novel environment-evoked transcriptional signature predicts reactivity in single dentate granule neurons. Nat Commun. 2018;9(1).
49. Simonetti M, Paldy E, Njoo C, Bali KK, Worzfeld T, Pitzer C, et al. The impact of Semaphorin 4C/Plexin-B2 signaling on fear memory via remodeling of neuronal and synaptic morphology. Mol Psychiatry. 2021;26(4).
50. Jitsuki-Takahashi A, Jitsuki S, Yamashita N, Kawamura M, Abe M, Sakimura K, et al. Activity-induced secretion of semaphorin 3A mediates learning. European Journal of Neuroscience. 2021;53(10).
51. Christian DL, Wu DY, Martin JR, Moore JR, Liu YR, Clemens AW, et al. DNMT3A Haploinsufficiency Results in Behavioral Deficits and Global Epigenomic Dysregulation Shared across Neurodevelopmental Disorders. Cell Rep. 2020 Nov;33(8):108416.
52. Li J, Pinto-Duarte A, Zander M, Cuoco MS, Lai CY, Osteen J, et al. Dnmt3a knockout in excitatory neurons impairs postnatal synapse maturation and increases the repressive histone modification H3K27me3. Elife. 2022 May 23;11.
53. Wu H, Coskun V, Tao J, Xie W, Ge W, Yoshikawa K, et al. Dnmt3a-Dependent Nonpromoter DNA Methylation Facilitates Transcription of Neurogenic Genes. Science (1979). 2010 Jul 23;329(5990):444–8.
54. Jiang J, Peng Y, He Z, Wei L, Jin W, Wang X, et al. Intrahippocampal injection of Cortistatin-14 impairs recognition memory consolidation in mice through activation of sst 2 , ghrelin and GABA A/B receptors. Brain Res. 2017 Jul;1666:38–47.
55. Xie R, Wang Z, Liu T, Xiao R, Lv K, Wu C, et al. AAV Delivery of shRNA Against TRPC6 in Mouse Hippocampus Impairs Cognitive Function. Front Cell Dev Biol. 2021 Jul 13;9.
56. Gøtzsche CR, Woldbye DPD. The role of NPY in learning and memory. Neuropeptides. 2016 Feb;55:79–89.
57. Cao L, Jiao X, Zuzga DS, Liu Y, Fong DM, Young D, et al. VEGF links hippocampal activity with neurogenesis, learning and memory. Nat Genet. 2004 Aug 18;36(8):827–35.
58. Kolodkin AL, Tessier-Lavigne M. Mechanisms and Molecules of Neuronal Wiring: A Primer. Cold Spring Harb Perspect Biol. 2011 Jun 1;3(6):a001727–a001727.
59. Wang Q, Chiu SL, Koropouli E, Hong I, Mitchell S, Easwaran TP, et al. Neuropilin-2/PlexinA3 Receptors Associate with GluA1 and Mediate Sema3F-Dependent Homeostatic Scaling in Cortical Neurons. Neuron. 2017 Dec;96(5):1084-1098.e7.
60. Sahay A, Kim CH, Sepkuty JP, Cho E, Huganir RL, Ginty DD, et al. Secreted Semaphorins Modulate Synaptic Transmission in the Adult Hippocampus. The Journal of Neuroscience. 2005 Apr 6;25(14):3613–20.

61. Sae-Lee C, Barrow TM, Colicino E, Choi SH, Rabanal-Ruiz Y, Green D, et al. Genomic targets and selective inhibition of DNA methyltransferase isoforms. Clin Epigenetics. 2022 Dec 20;14(1):103.
62. Jurkowska RZ, Jeltsch A. Enzymology of Mammalian DNA Methyltransferases. In 2016. p. 87–122.
63. Holz-Schietinger C, Reich NO. RNA modulation of the human DNA methyltransferase 3A. Nucleic Acids Res. 2012 Sep;40(17):8550–7.
64. Mohammad F, Pandey GK, Mondal T, Enroth S, Redrup L, Gyllensten U, et al. Long noncoding RNA-mediated maintenance of DNA methylation and transcriptional gene silencing. Development. 2012 Aug 1;139(15):2792–803.
65. Watanabe T, Tomizawa S ichi, Mitsuya K, Totoki Y, Yamamoto Y, Kuramochi-Miyagawa S, et al. Role for piRNAs and Noncoding RNA in de Novo DNA Methylation of the Imprinted Mouse *Rasgrf1* Locus. Science (1979). 2011 May 13;332(6031):848–52.
66. Di Ruscio A, Ebralidze AK, Benoukraf T, Amabile G, Goff LA, Terragni J, et al. DNMT1-interacting RNAs block gene-specific DNA methylation. Nature. 2013 Nov 9;503(7476):371–6.
67. Savell KE, Gallus NVN, Simon RC, Brown JA, Revanna JS, Osborn MK, et al. Extra-coding RNAs regulate neuronal DNA methylation dynamics. Nat Commun. 2016 Jul 7;7(1):12091.
68. Ooi SKT, Qiu C, Bernstein E, Li K, Jia D, Yang Z, et al. DNMT3L connects unmethylated lysine 4 of histone H3 to de novo methylation of DNA. Nature. 2007 Aug;448(7154):714–7.
69. Suetake I, Mishima Y, Kimura H, Lee YH, Goto Y, Takeshima H, et al. Characterization of DNA-binding activity in the N-terminal domain of the DNA methyltransferase Dnmt3a. Biochemical Journal. 2011 Jul 1;437(1):141–8.
70. Pohodich AE, Zoghbi HY. Rett syndrome: disruption of epigenetic control of postnatal neurological functions. Hum Mol Genet. 2015 Oct 15;24(R1):R10–6.
71. De Jager PL, Srivastava G, Lunnon K, Burgess J, Schalkwyk LC, Yu L, et al. Alzheimer's disease: early alterations in brain DNA methylation at ANK1, BIN1, RHBDF2 and other loci. Nat Neurosci. 2014 Sep 17;17(9):1156–63.
72. Feng J, Nestler EJ. Epigenetic mechanisms of drug addiction. Curr Opin Neurobiol. 2013 Aug;23(4):521–8.
73. Nestler EJ, Peña CJ, Kundakovic M, Mitchell A, Akbarian S. Epigenetic Basis of Mental Illness. The Neuroscientist. 2016 Oct 9;22(5):447–63.
74. Denk F, McMahon SB. Chronic Pain: Emerging Evidence for the Involvement of Epigenetics. Neuron. 2012 Feb;73(3):435–44.

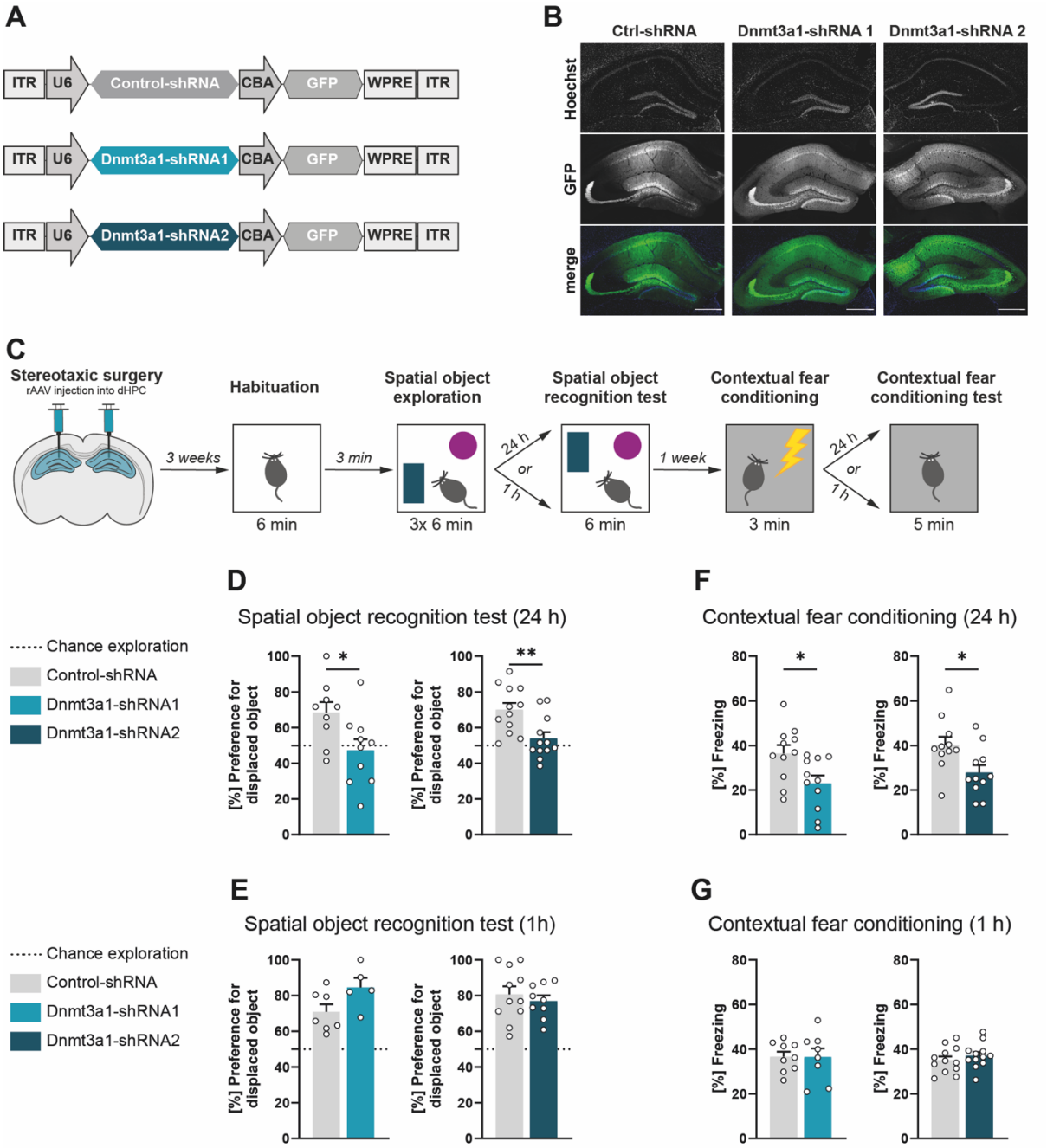

Figure 1: Reduced hippocampal Dnmt3a1 levels impair memory formation. (**A**) Schematic representation of viral constructs. (**B**) Representative images of the dorsal hippocampus of mice infected with Control-shRNA, Dnmt3a1-shRNA1 or Dnmt3a1-shRNA2. Scale bar: 100 µm. (**C**) Schematic representation of experimental design. (**D, E**) Long-term (D) or short-term (E) spatial object recognition memory of mice expressing Control-shRNA (n=7-12), Dnmt3a1-shRNA1 (n=5-10) or Dnmt3a1-shRNA2 (n=9-12). Dashed lines represent equal preference for either object (chance exploration). *p<0.05, **p<0.01 by two-tailed,

830 unpaired t-test. (**F, G**) Long-term (F) or short-term (G) contextual fear memory of mice
831 expressing Control-shRNA (n=9-11), Dnmt3a1-shRNA1 (n=8-11) or Dnmt3a1-shRNA2 (n=11-
832 13). *p<0.05 by two-tailed, unpaired t-test.

833

834

835

836

837

838

839

840

841

842

843

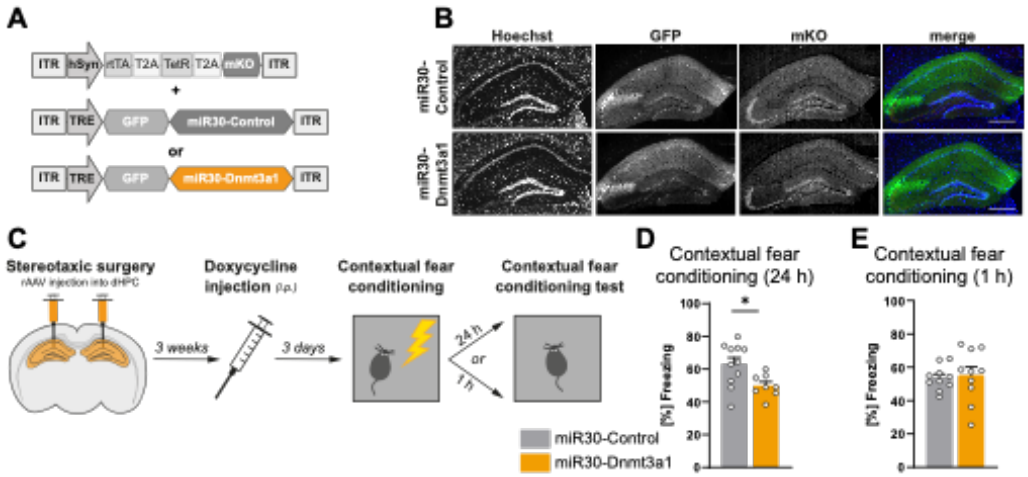

Figure 2: Temporally-restricted Dnmt3a1 knockdown impairs memory consolidation. (**A**) Schematic representation of the viral constructs encoding the TetON-based system. The driver construct expresses under the hSyn promoter the Tet repressor (TetR), the reverse tetracycline-controlled transactivator (rtTA) and the infection marker Kusabira Orange (mKO). The Tet response element (TRE)-dependent construct contains the TRE promoter driving the miR30-based shRNA cassettes. In the absence of doxycycline, TRE is inhibited by TetR which results in suppression of the miR30 system. In the presence of doxycycline, TetR loses its affinity thus enabling rtTA to bind to TRE and activate the expression of the miR30 system. (**B**) Representative images of the dHPC of mice infected with rAAVs expressing the miR30-Control shRNA or miR30- Dnmt3a1-shRNA2 sequence. Scale bar: 100 µm. (**C**) Schematic representation of experimental design. (**D, E**) Long-term (D) or short-term (E) contextual fear memory of mice expressing miR30-Control shRNA (n=12-17) or miR30-Dnmt3a1 shRNA (n=10-14). *p<0.05, by two-tailed, unpaired t-test.

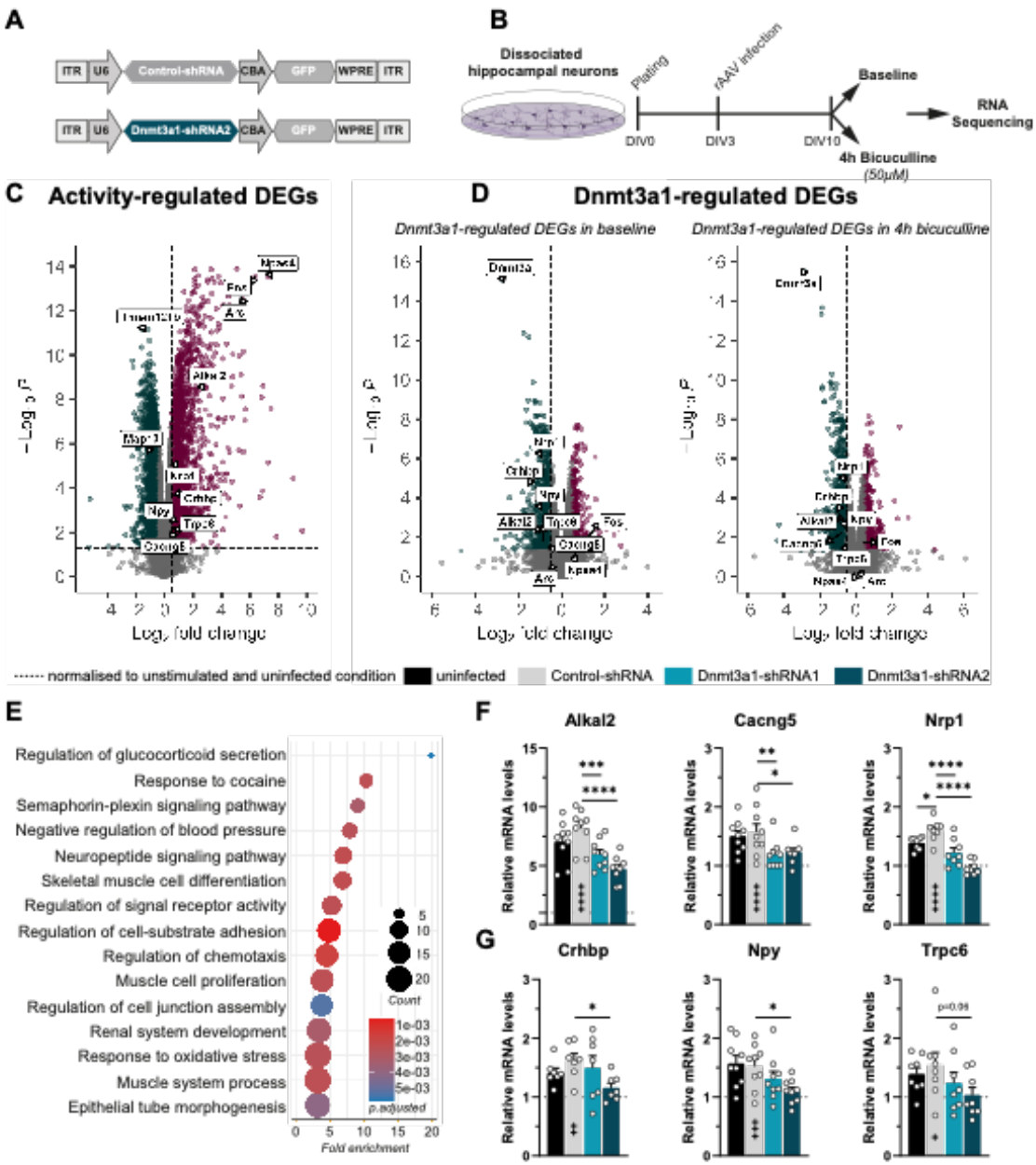

862

863 **Figure 3: Dnmt3a1 regulates transcription of genes involved in synaptic plasticity**
864 **processes.** (**A**) Schematic representation of viral constructs. (**B**) Experimental design used
865 to identify activity-regulated genes whose expression is altered upon Dnmt3a1 reduction. DIV:
866 Day *in-vitro*. (**C**) Volcano plot of differentially expressed genes (DEGs) in control condition
867 (infected with rAAVs expressing Control-shRNA) in response to neuronal activity via
868 Bicuculline treatment; n=4 independent neuronal preparation per condition. Log2 fold change
869 cut-off: ± 0.5; adjusted p-value cut-off: 0.05. (**D**) Volcano plot of DEGs upon infection with

870 Control-shRNA or Dnmt3a1-shRNA2 in baseline condition or in stimulated condition (4h
871 bicuculline); n=4 independent neuronal preparation per condition. Log2 fold change cut-off: ±
872 0.5; adjusted p-value cut-off: 0.05. (**E**) GO-Term analysis of overlapping genes between
873 activity-regulated and Dnmt3a1-regulated DEGs. Dot plot illustrates Top 15 GO term
874 enrichment of biological processes. (**F**) qRT-PCR analysis of *Alkal2*, *Cacng5*, *Nrp1* expression
875 levels in hippocampal cultures infected with Control–shRNA or Dnmt3a1-shRNA1 or -shRNA2
876 and stimulated 4h with Bicuculline. Expression levels were normalised to the uninfected
877 control in baseline conditions (dashed line); (n=8-9 independent neuronal cultures). *$p<0.05$,
878 ***$p\leq0.001$, ****$p\leq0.0001$ by one-way ANOVA test followed by Sidak's multiple comparisons
879 test(**G**) qRT-PCR analysis of *Crhbp*, *Npy*, *Trpc6* expression levels in hippocampal-cultured
880 cells infected with Control–shRNA or Dnmt3a1-shRNA1 or -shRNA2 and stimulated 4h with
881 Bicuculline. Expression levels were normalised to the uninfected control in baseline conditions
882 (dashed line); (n=7-9 independent neuronal cultures). *$p<0.05$, **$p\leq0.01$, ns: not significant by
883 one-way ANOVA test followed by Sidak's multiple comparisons test. Control-shRNA 4h
884 bicuculline versus unstimulated: $^{+}p<0.05$, $^{++}p<0.01$, $^{+++}p\leq0.001$, $^{++++}p\leq0.0001$ by one-way
885 ANOVA test followed by Sidak's multiple comparisons test.

886
887

888

889

890

891

892

893

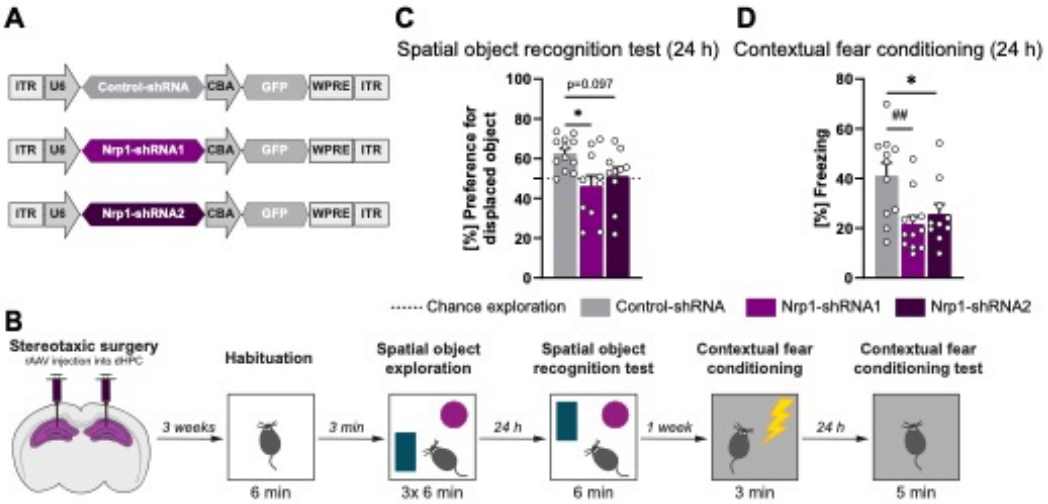

Figure 4: Hippocampal Neuropilin-1 is required for memory formation. (**A**) Schematic representation of viral constructs. (**B**) Schematic representation of experimental design. (**C**) Long-term spatial object recognition memory of mice expressing Control-shRNA (n=12), Nrp1-shRNA1 (n=10) or Nrp1-shRNA2 (n=10). Dashed lines represent equal preference for either object (chance exploration). *p<0.05 by one-way ANOVA test followed by Dunnett's multiple comparisons test. (**D**) Long-term contextual fear memory of mice infected with rAAVs expressing Control-shRNA (n=11), Nrp1-shRNA1 (n=12) or Nrp11-shRNA2 (n=10). *p<0.05 by one-way ANOVA test followed by Dunnett's multiple comparisons test. $^{\#\#}$p≤0.01 by Kruskal-Wallis test followed by Dunn's multiple comparisons test.

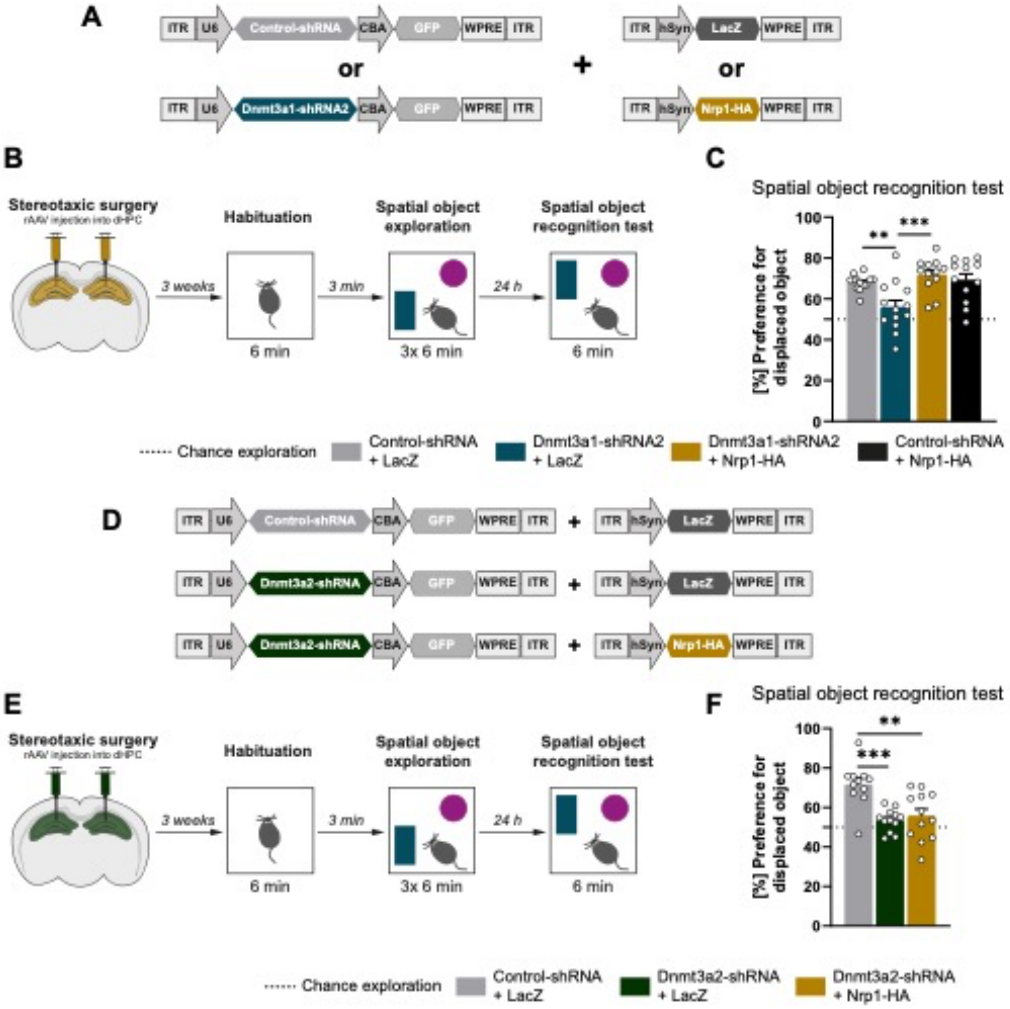

Figure 5: Neuropilin-1 rescues Dnmt3a1-, but not Dnmt3a2-, dependent memory impairments. (**A**) Schematic representation of viral constructs. (**B**) Schematic representation of experimental design. (**C**) Long-term spatial object recognition memory of mice expressing Control-shRNA + LacZ (n=13), Dnmt3a1-shRNA2 + LacZ (n=13), Dnmt3a1-shRNA2 + Nrp1-HA (n=12) or Control-shRNA + Nrp1-HA (n=12). Dashed lines represent equal preference for either object (chance exploration). **p≤0.01, ***p≤0.001 by one-way ANOVA test followed by Sidak's multiple comparisons test. (**D**) Schematic representation of viral constructs. (**E**) Schematic representation of experimental design. (**F**) Long-term spatial object recognition memory mice expressing Control-shRNA + LacZ (n=11), Dnmt3a2-shRNA + LacZ (n=12) or Dnmt3a2-shRNA + Nrp1-HA (n=12). Dashed lines represent equal preference for either object

921 (chance exploration). **p≤0.01, ***p≤0.001 by one-way ANOVA test followed by Sidak's
922 multiple comparisons test.

923

924

925

926

927